Biocompatible Nanoparticles with Aggregation-Induced Emission Characteristics as Far-Red/Near-Infrared Fluorescent Bioprobes for In Vitro and In Vivo Imaging Applications

Wei Qin, Dan Ding, Jianzhao Liu, Wang Zhang Yuan, Yong Hu, Bin Liu, and Ben Zhong Tang**

Light emission of 2-(2,6-bis((*E*)-4-(diphenylamino)styryl)-4*H*-pyran-4-ylidene) malononitrile (TPA-DCM) is weakened by aggregate formation. Attaching tetraphenylethene (TPE) units as terminals to TPA-DCM dramatically changes its emission behavior: the resulting fluorogen, 2-(2,6-bis((*E*)-4-(phenyl(4′-(1,2,2-triphenylvinyl)-[1,1′-biphenyl]-4-yl)amino)styryl)-4*H*-pyran-4-ylidene) malononitrile (TPE-TPA-DCM), is more emissive in the aggregate state, showing the novel phenomenon of aggregation-induced emission (AIE). Formulation of TPE-TPA-DCM using bovine serum albumin (BSA) as the polymer matrix yields uniformly sized protein nanoparticles (NPs) with high brightness and low cytotoxicity. Applications of the fluorogen-loaded BSA NPs for in vitro and in vivo far-red/near-infrared (FR/NIR) bioimaging are successfully demonstrated using MCF-7 breast-cancer cells and a murine hepatoma-22 (H_{22})-tumor-bearing mouse model, respectively. The AIE-active fluorogen-loaded BSA NPs show an excellent cancer cell uptake and a prominent tumor-targeting ability in vivo due to the enhanced permeability and retention effect.

1. Introduction

The emergence of non-invasive, live-animal fluorescence imaging technology has opened new avenues for the development of cancer diagnosis and therapeutics.[1] Fluorescence imaging probes with intense emission in the far-red/near-infrared (FR/NIR) region (>650 nm) are attracting increasing attention due to their capability of overcoming the interferences of optical absorption, light scattering and autofluorescence of biological media.[2] To date, a large variety of materials, including organic dyes,[3] fluorescent proteins[4] and inorganic quantum dots (QDs),[5] has been extensively studied for the purpose of FR/NIR fluorescence imaging. Organic dyes and fluorescent proteins, however, suffer from limited molar absorptivity and low photobleaching thresholds,[6] while inorganic QDs are highly cytotoxic in an oxidative environment:[7] this has greatly limited the scope of their in vitro and in vivo applications. Exploration of novel FR/NIR fluorescent probes with a high biological compatibility, strong photobleaching resistance, and efficient light emission is highly desirable for live-animal imaging.

Fluorescent nanoparticles (NPs), such as organic-fluorophore-loaded NPs, have recently emerged as a new generation of nanoprobes for bioimaging. They show such advantages as synthetic versatility, low cytotoxicity, high photostability and facile surface functionalization for specific targeting.[8] For practical applications, brightly emissive NPs are desirable for high-contrast imaging. In the ideal case, the brightness of fluorophore-doped NPs should be proportional to the number of encapsulated dye molecules. However, at high loading contents, π-conjugated fluorophores are prone to aggregation. Aggregate formation often quenches light emission due to π–π stacking and other non-radiative pathways, a common photophysical phenomenon notoriously known as aggregation-caused quenching (ACQ). The ACQ effect has been a thorny hurdle in the fabrication of NPs with high brightness.[9] We have recently developed a novel class of organic luminogens with an extraordinary aggregation-induced-emission (AIE) feature,[10,11] which is exactly opposite to the above-mentioned ACQ system. These luminogens, with tetraphenylethene (TPE) being a typical example, are non-emissive in dilute solution but are induced to luminesce intensely when aggregated through a mechanism of the restriction of intramolecular rotation.[11] The development of these unique AIE luminogens sweeps away our concerns of emission quenching induced by a high fluorophore loading in NPs.

The AIE fluorogens that have been developed so far are largely blue and green emitters. Although a fluorescence quantum yield (Φ_F) of almost unity has been realized in some AIE systems in

W. Qin, Dr. J. Liu, Dr. W. Z. Yuan, Prof. B. Z. Tang
Department of Chemistry
The Hong Kong University of Science & Technology
Clear Water Bay, Kowloon
Hong Kong, China
E-mail: tangbenz@ust.hk
Dr. D. Ding, Prof. B. Liu
Department of Chemical and Biomolecular Engineering
National University of Singapore, 117576, Singapore
E-mail: cheliub@nus.edu.sg
Y. Hu
National Laboratory of Solid-State Microstructure
Department of Material Science and Engineering
Nanjing University
Nanjing 210093, China
Prof. B. Liu, Prof. B. Z. Tang
Institute of Materials Research Engineering
3 Research Link, 117602, Singapore

DOI: 10.1002/adfm.201102191

the aggregate state,[11] they are not ideally suited to bioimaging applications due to their light emission in the short-wavelength region. Many red emitters (e.g., 2-(4*H*-pyran-4-ylidene)malononitrile (DCM)) are known, but they are unfortunately not so emissive in the solid state due to the involved ACQ process. We recently developed a structural design strategy for transforming conventional ACQ chromophores to efficient solid emitters by covalent integration with AIE luminogens.[12] In general, the resultant adducts inherit the AIE feature and display a red-shifted emission, in comparison with those of their ACQ parents, due to the extension in the electronic conjugation. As FR/NIR chromophores generally possess planar molecular structures with a weak emission in the solid state, our new strategy should enable us to develop efficient FR/NIR emitters by simply modifying the conventional ACQ chromophores with AIE fluorogens. As a proof of concept, we chose a triphenylamine (TPA)-modified DCM derivative, 2-(2,6-bis((*E*)-4-(diphenylamino)styryl)-4*H*-pyran-4-ylidene)malononitrile (TPA-DCM; **Scheme 1**), which shows poor FR emission in the aggregate state, as a model ACQ chromophore. Two TPE units were introduced to the periphery of the TPA-DCM core to generate a 2-(2,6-bis((*E*)-4-(phenyl(4′-(1,2,2-triphenylvinyl)-[1,1′-biphenyl]-4-yl)amino)styryl)-4*H*-pyran-4-ylidene)malononitrile (TPE-TPA-DCM) adduct that is AIE active, emitting bright FR/NIR light in the aggregate state. Its excitation and emission profiles match well with commercial laser sources and fluorescence-imaging systems, making it promising for bioimaging applications.

In this contribution, we report the synthesis of TPE-TPA-DCM, the fabrication of its NPs, and the application of the NPs for in vitro and in vivo imaging. Bovine serum albumin (BSA) was selected as the polymer matrix for formulating NPs loaded with TPE-TPA-DCM because albumin is biocompatible, non-antigenic and clinically utilized.[13] In addition, BSA-based NPs have been reported to accumulate preferentially in tumors through the enhanced permeability and retention (EPR) effect, known as "passive" targeting.[14] As there have been almost no previous reports on the application of AIE-active NPs in live-animal fluorescence imaging via intravenous administration, the successful demonstration of the AIE-active fluorogen-loaded BSA NPs for FR/NIR imaging of targeted tumors in living bodies should inspire more exciting research in this emerging field for cancer diagnosis.

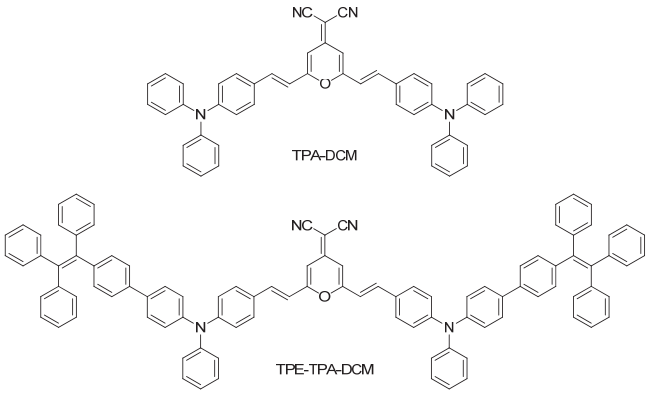

Scheme 1. Chemical structures of TPA-DCM and TPE-TPA-DCM.

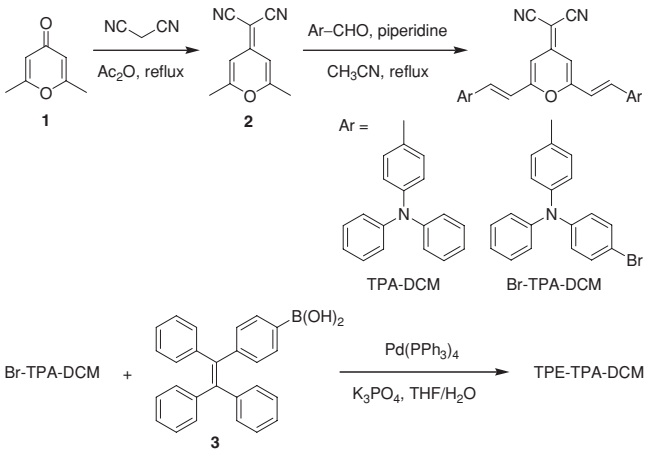

Scheme 2. Synthetic routes to TPA-DCM and TPE-TPA-DCM.

2. Results and Discussion

2.1. Synthesis and Characterization of TPE-TPA-DCM

TPA-DCM and TPE-TPA-DCM were prepared according to the synthetic routes shown in **Scheme 2**. 2-(2,6-Dimethyl-4*H*-pyran-4-ylidene)malononitrile (**2**) was prepared in a 73% yield from 2,6-dimethyl-4-pyrone (**1**) according to the synthetic procedures published by Wood.[15] Knoevenagel condensation reactions of **2** with TPA-containing aldehydes[16] gave TPA-DCM and Br-TPA-DCM adducts in yields of over 70%. TPE-TPA-DCM was obtained in a 60% yield by Suzuki coupling between the Br-TPA-DCM and 4-(1,2,2-triphenylvinyl)phenylboronic acid (**3**),[17] using tetrakis(triphenylphosphane)palladium(0) ($Pd(PPh_3)_4$) as a catalyst, under basic conditions.

The TPE-TPA-DCM was isolated by column chromatography followed by recrystallization. The purified product was characterized using standard spectroscopic methods. Its numerical spectral data are summarized in the Experimental Section and examples of its spectra (Figure S1–S3, Supporting Information) are shown. The coupling constant of its vinyl protons in the ^{1}H-NMR spectrum was 16 Hz, proving that it possesses a *trans* conformation. Formation of the *trans* isomer was favored in the reaction due to the thermodynamic stability of the *trans* conformation and the steric hindrance hampering the formation of the *cis* structure. The NMR spectroscopy peaks of the minor *cis* isomer were absent, possibly because any *cis* isomer was removed by the recrystallization process during product purification.

TPA-DCM is composed of two TPA donor (D) units and one DCM acceptor (A) unit, with the latter being a well-known ACQ chromophore. The absorption spectrum of its tetrahydrofuran (THF) solution has a peak at ≈487 nm, and it has a molar absorptivity of 7.1×10^4 L mol^{-1} cm^{-1}. Such D-A fluorophores often show the photophysical phenomenon named twisted intramolecular charge transfer (TICT), which is featured with a red-shifted emission color and a decreased emission intensity with increasing solvent polarity.[18] We measured the photoluminescence (PL) spectra of TPA-DCM in THF/water mixtures, with different water fractions (f_w), which enabled fine-

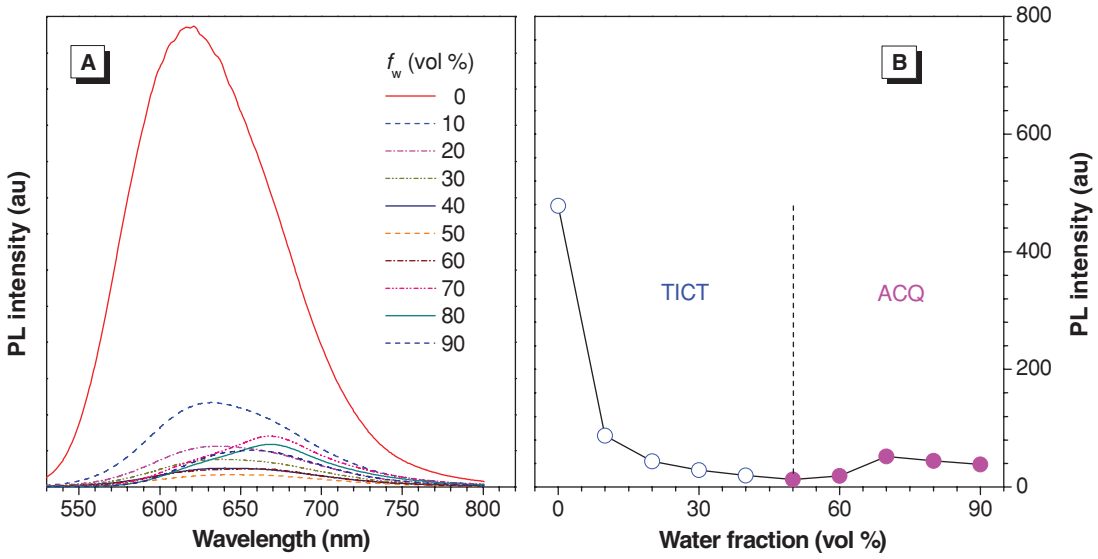

Figure 1. a) PL spectra of TPA-DCM in THF/water mixtures with different water fractions (f_w). b) Plot of peak intensity of TPA-DCM versus water fraction in the aqueous mixtures. [TPA-DCM] = 10×10^{-6} M; λ_{ex} = 480 nm.

tuning of the solvent polarity and the extent of solute aggregation. The pure THF solution of TPA-DCM had an intense red fluorescence with an emission maximum at 620 nm, which was dramatically quenched when a small amount of water was added, as evidenced by its weak emission in the THF/water mixtures with $f_w \leq 50$ vol% (**Figure 1**). Meanwhile, the emission maximum was bathochromically shifted to ≈670 nm. This is a typical TICT effect arising from the increased solvent polarity. When more water ($f_w > 50$ vol%) was added, the TPA-DCM molecules formed nanoaggregates. Although a hydrophobic environment was created inside the nanoaggregates and the TICT effect should be alleviated,[18] the fluorescence did not recover because of the prevailing ACQ effect.

TPE is a paradigm of AIE luminogens. According to our recently developed structural-design principle,[12] attaching TPE units to TPA-DCM should endow the resultant adduct, TPE-TPA-DCM, with an AIE attribute, whilst retaining the TICT features of its parent form, TPA-DCM.[18] This proved to be the case. As shown in **Figure 2**, the TPE-TPA-DCM exhibited an emission maximum at 633 nm in THF, which was red-shifted 13 nm from that of TPA-DCM. With a gradual addition of water into the THF, the emission of the TPE-TPA-DCM was dramatically weakened and the emission color was bathochromically shifted due to the increase in the solvent polarity and the transformation to the TICT state. The light emission was invigorated from $f_w \approx 50$ vol% and was intensified with a further increase

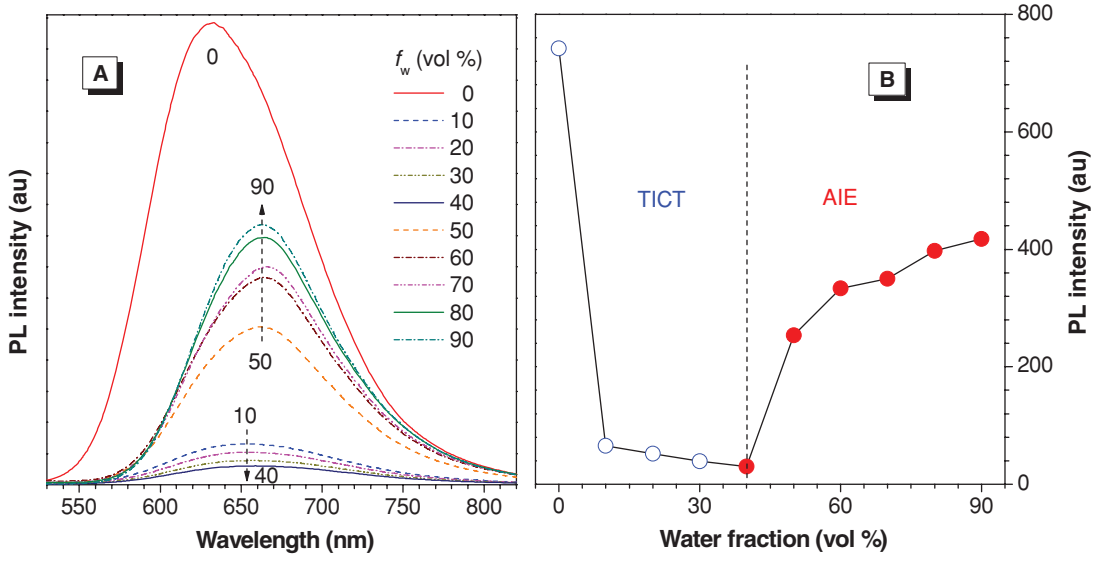

Figure 2. a) PL spectra of TPE-TPA-DCM in THF/water mixtures with different water fractions (f_w). b) Plot of peak intensity of TPE-TPA-DCM versus water fraction in the aqueous mixtures. [TPE-TPA-DCM] = 10×10^{-6} M; λ_{ex} = 480 nm.

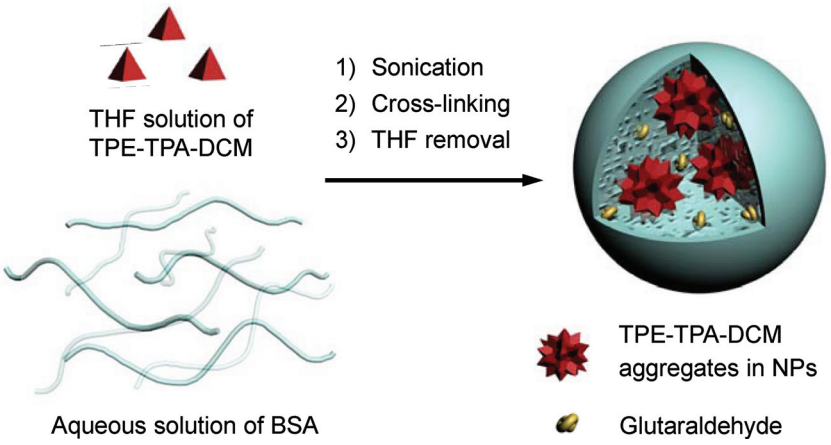

Scheme 3. Schematic illustration of the fabrication of BSA NPs loaded with TPE-TPA-DCM.

in f_w. Meanwhile, the emission maximum was gradually red-shifted to ≈660 nm when f_w reached 90 vol%. These data verify our anticipation that TPE-TPA-DCM is a luminogen with both TICT and AIE characteristics.

2.2. Fabrication and Characterization of BSA NPs Loaded with TPE-TPA-DCM

The procedure for the preparation of the fluorogen-loaded BSA NPs is illustrated in **Scheme 3**. Upon addition of the TPE-TPA-DCM solution in THF to the aqueous solution of BSA, the TPE-TPA-DCM molecules aggregate and entangle with the hydrophobic domains of the BSA chains. The BSA gradually phase-separates, accompanying its hybridization with the hydrophobic fluorogen. The fluorogen-loaded BSA NPs form instantly upon sonication. The BSA matrix is knitted together by glutaraldehyde, an amine-reactive homo-bifunctional cross-linker. The THF is then removed and the cross-linked NPs are further purified by filtration through a 0.45 μm microfilter, followed by washing with Milli-Q water. The zeta potential of the purified NPs was −29 mV in aqueous suspension, suggesting that the NPs are stabilized by outer layers of ionized carboxylic groups.

Table 1 shows the encapsulation efficiencies (EE) and average sizes of the AIE-active fluorogen-loaded NPs prepared at different feeding ratios of TPE-TPA-DCM. The fluorogen loading increased with an increase in the fluorogen feeding. The EE of the fluorogen was >85 wt% when the TPE-TPA-DCM feeding ratio was <1 wt%, while a decrease in the EE was observed when the fluorogen feeding ratio was increased to >1 wt%. The average size of the pure BSA NPs without AIE-fluorogen encapsulation was 97.1 nm, with a narrow size distribution or polydispersity (PDI = 0.065). The average size of the BSA NPs increased from 98.8 nm to 148.1 nm when the fluorogen loading was increased from 0.25 wt% to 3.07 wt%. In comparison, the average size of the bare TPE-TPA-DCM NPs prepared from an aqueous mixture with f_w = 90 vol% (cf., Figure 2) was measured to be 307.3 nm by laser-light scattering (LLS) with a broad size distribution (PDI = 0.279).

Transmission electron microscopy (TEM) and field-emission scanning electron microscopy (FE-SEM) images of the fluorogen-loaded BSA NPs with a 0.86 wt% loading of TPE-TPA-DCM are shown in **Figure 3** as examples. The images indicate that the AIE-active fluorogen-loaded NPs had a spherical shape and a smooth surface with an almost uniform size of around 90 nm. This size is smaller than that obtained from the LLS measurement (124.7 nm) due to a shrinkage of the BSA NPs in the ultra-dry state under the high vacuum in the TEM and FE-SEM chambers.

Figure 4 shows the absorption and emission spectra of the AIE-active fluorogen-loaded BSA NPs with a 0.86 wt% fluorogen loading and of the bare TPE-TPA-DCM NPs suspended in water. The fluorogen-loaded BSA NPs show two absorption maxima at 360 and 505 nm, while those of the bare TPE-TPA-DCM NPs are slightly blue-shifted, appearing at 359 and 497 nm. The emission maximum of the fluorogen-loaded BSA NPs is located at 668 nm, similar to that of the bare TPE-TPA-DCM NPs in water. The emission intensity of the fluorogen-loaded BSA NPs increased almost linearly with increasing fluorogen loading within the studied range (**Figure 5**). The Φ_F values of the fluorogen-loaded BSA NPs in water were measured using Rhodamine 6G in ethanol as the standard. The Φ_F initially increased rapidly and then slowly with increasing fluorogen loading. It eventually reached a value of ≈12% at a fluorogen loading of 3.07 wt%.

Table 1. Characteristics of the BSA NPs loaded with TPE-TPA-DCM.

TPE-TPA-DCM feeding ratio[a] [wt%]	TPE-TPA-DCM loading ratio[b] [wt%]	Encapsulation efficiency [wt%]	Size[c] [nm] (PDI)[d]
0	0		97.1 (0.065)
0.25	0.25	100	98.8 (0.089)
0.5	0.49	98.7	124.8 (0.125)
1.0	0.86	85.6	124.7 (0.110)
2.5	1.87	74.8	141.3 (0.180)
5.0	3.07	61.4	148.1 (0.161)

[a]The ratio of the weight of TPE-TPA-DCM to that of BSA in the feed mixture; [b]The ratio of the weight of the loaded TPE-TPA-DCM to that of the BSA matrix in the NPs; [c]Average diameter of the NPs measured by laser light scattering (LLS); [d]Polydispersity index (PDI).

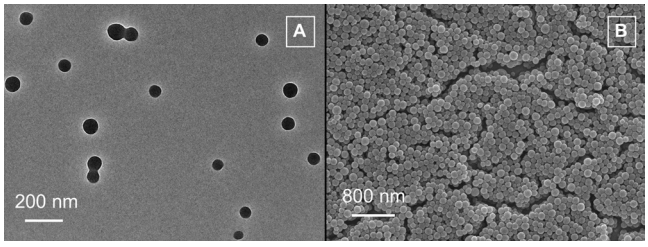

Figure 3. a,b) TEM (a) and FE-SEM (b) images of the AIE-active fluorogen-loaded BSA NPs.

Nanomaterials with an average diameter of ≈100 nm have been reported to show prolonged blood circulation in vivo, resulting in their accumulation in tumors through the EPR process.[19] In the following in vitro and in vivo imaging experiments, AIE-active fluorogen-loaded BSA NPs with a TPE-TPA-DCM loading ratio of 0.86 wt% were used, due to their proper particle size, relatively high EE and good quantum yield.

2.3. In Vitro Cellular Imaging

The application of the fluorogen-loaded BSA NPs for in vitro cellular imaging was studied using confocal laser scanning microscopy (CLSM). After incubation with the BSA-NP suspension (0.4×10^{-6} M TPE-TPA-DCM) for 2 h at 37 °C in the culture medium, MCF-7 breast-cancer cells were fixed and the cell nuclei were stained with 4′,6-diamidino-2-phenylindole (DAPI). The cells were imaged by CLSM with a 488 nm laser excitation and the fluorescent signals were collected at above 650 nm for the NPs and 560 nm for DAPI, respectively. As shown in **Figure 6**A, an intense red fluorescence was observed in the cellular cytoplasms and was further confirmed by the corresponding 3D CLSM image (Figure S4, Supporting Information).

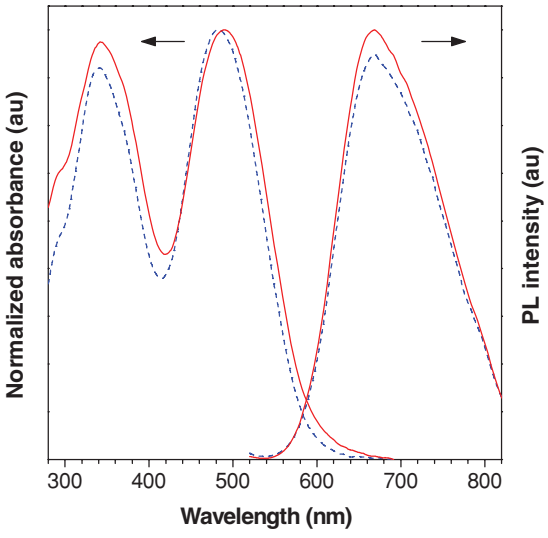

Figure 4. Normalized UV–vis absorption and PL emission spectra of the fluorogen-loaded BSA NPs (with TPE-TPA-DCM loading of 0.86%; red) and the bare TPE-TPA-DCM NPs (blue) in water.

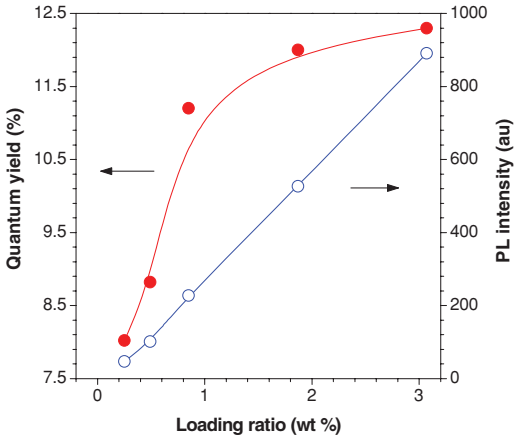

Figure 5. Changes in the quantum yield and PL intensity with the weight ratio of TPE-TPA-DCM in the fluorogen-loaded BSA NPs.

Figure 6B shows a CLSM image of MCF-7 cells after incubation with bare TPE-TPA-DCM NPs (0.4×10^{-6} M) for 2 h at 37 °C. Only a few bare NPs were observed in the cytoplasm with a weak fluorescence. The internalization of the bare fluorogen NPs in the cytoplasm was also confirmed by a 3D CLSM image (Figure S5, Supporting Information). The homogeneous distribution of the AIE-active fluorogen-loaded BSA NPs in the cytoplasms, with a stronger fluorescence compared with the bare TPE-TPA-DCM NPs, suggests that BSA as the encapsulation matrix efficiently enhanced the intracellular uptake of the formulated NPs. These results manifest that the fluorogen-loaded BSA NPs are effective FR/NIR fluorescent bioprobes for cellular imaging with a high fluorescence contrast. In addition, the photostabilities of the AIE-fluorogen-loaded BSA NPs and fluorescein isothiocyanate in the MCF-7 cancer cells were also studied under continuous laser scanning upon excitation at 488 nm (**Figure 7**). The AIE-fluorogen-loaded NPs showed a decrease of less than 10% in their fluorescence intensity after continuous laser exposure for 10 min, which was much better than that of fluorescein isothiocyanate under the same conditions. These data indicate the good photostability of the AIE-fluorogen-loaded BSA NPs in a biological environment, which meets the requirements for bioimaging applications.

The in vitro cytotoxicity of the fluorogen-loaded BSA NPs against MCF-7 breast-cancer cells was investigated using a

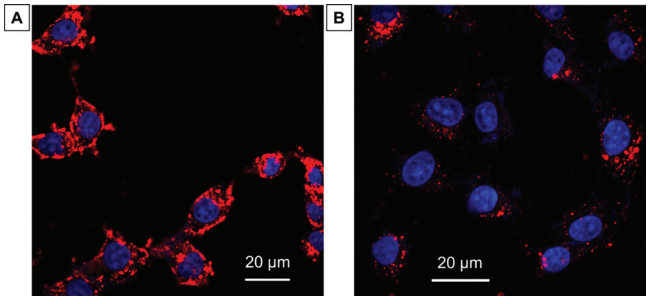

Figure 6. a,b) CLSM images of MCF-7 breast cancer cells after incubation with fluorogen-loaded BSA NPs (with a fluorogen loading of 0.86%) (a) and bare TPE-TPA-DCM NPs (b) for 2 h at 37 °C. [TPE-TPA-DCM] = 0.4×10^{-6} M.

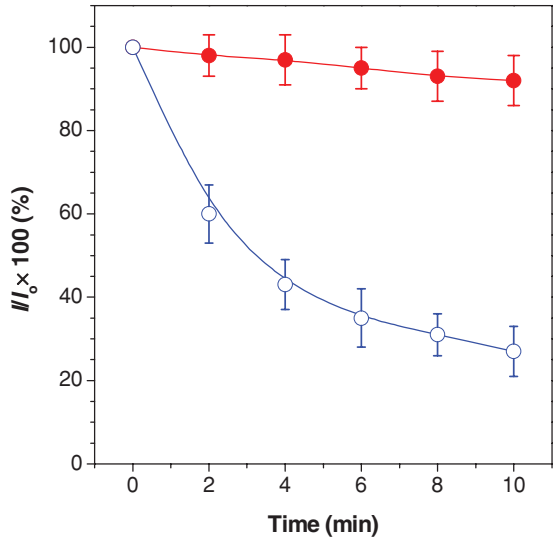

Figure 7. Photostability comparison between TPE-TPA-DCM-loaded BSA NPs (red) and fluorescein isothiocyanate (blue) in MCF-7 cancer cells upon continuous excitation at 488 nm (1.25 mW) for 0 to 10 min. I_0 is the initial fluorescence intensity and I is the fluorescence intensity of the sample after continuous exposure for designated time intervals.

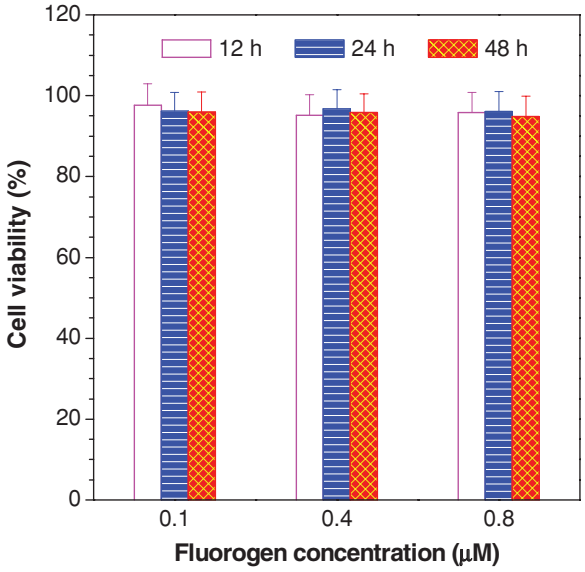

Figure 8. Metabolic viability of MCF-7 breast cancer cells after incubation with fluorogen-loaded BSA NPs at various fluorogen concentrations for 12, 24, and 48 h.

3-(4,5-dimethylthiazol-2-yl)-2,5-diphenyltetrazolium bromide (MTT) cell-viability assay. **Figure 8** shows the cell viability after incubation with the NP suspension at fluorogen concentrations of 0.1×10^{-6}, 0.4×10^{-6}, and 0.8×10^{-6} M for 12, 24, and 48 h, respectively. Cell viabilities of more than 95% were observed for all the fluorogen concentrations within the tested periods of time, indicating that the AIE-active fluorogen-loaded BSA NPs had low cytotoxicity or good biocompatibility. The low cytotoxicity makes the NPs promising for bioimaging applications and superior to QDs, which are well-known for their concentration-dependent cytotoxicity.[7b]

2.4. In Vivo Imaging on a Tumor-Bearing Mouse Model

The fluorogen-loaded BSA NPs were also examined for in vivo FR/NIR bioimaging applications, employing the non-invasive live-animal fluorescence imaging technique. Murine hepatoma-22 (H_{22}) -transplanted tumor-bearing ICR mice were used as model animals, which were established by subcutaneously inoculating the H_{22} cancer cells into the left axillae of the mice. After intravenous injection with the fluorogen-loaded BSA NPs, the H_{22}-tumor-bearing mice were imaged using a Maestro EX in vivo fluorescence-imaging system. The mouse autofluorescence was removed by spectral unmixing using the Maestro software (Figure S6, Supporting Information). **Figure 9**A shows the time-dependent in vivo distribution profile and tumor accumulation of the AIE-fluorogen-loaded BSA NPs in the H_{22}-tumor-bearing mice. Clear tumor delineations with intense fluorescence were observed in the left axilla of the mouse at all of the imaging times, indicating an accumulation of the fluorogen-loaded BSA NPs in the tumor tissue. The capability of the fluorogen-loaded BSA NPs to illuminate the tumor tissue selectively with a high contrast may be associated with two factors. The first is that the AIE-active NPs accumulated in the tumor were highly fluorescent, while the second is the "passive" tumor-targeting ability by the EPR effect, which benefited from the uniform NP size of ≈100 nm.[19] Although strong fluorescence was also observed in the abdomen and liver areas of the same mouse at 3 h post-injection, it had almost completely disappeared after 28 h. This suggests that the AIE-fluorogen-loaded BSA NPs underwent uptake by the reticuloendothelial system (RES) organs, such as the liver and the spleen,[20] followed by facile excretion from the body through the biliary pathway,[21] which was further confirmed by the clear fluorescent signals observed in the collected feces. The clearance rate of the NPs within the tumors, however, was very slow, due to the lack of lymphatic drainage.[22] At 28 h post-injection, the uptake of the fluorogen-loaded BSA NPs in the tumor became prominent, in sharp contrast to the weak fluorescence signals in the other parts of the mouse body, demonstrating the promise of the NPs as FR/NIR fluorescent bioprobes for cancer diagnosis. The prominent EPR effect of the AIE-fluorogen-loaded BSA NPs was also demonstrated using ex vivo fluorescence imaging, which was performed on the excised tumor tissue, as well as the major organs, when the mice were sacrificed (**Figure 10**).

As a control, the mice intravenously injected with the bare TPE-TPA-DCM NPs at the same fluorogen concentration were imaged and analyzed. As shown in Figure 9B, the fluorescence intensities in the abdomen and liver areas of the mouse were much higher than in the tumor tissue at all of the tested time points. This is due to the fact that the bare TPE-TPA-DCM NPs had a relatively large average particle size (≈300 nm), most not being able to escape RES uptake.[19,23] As a consequence, accumulation of the bare fluorogen NPs in the tumors was limited and the tumor imaging showed poor fluorescence contrast. In comparison, H_{22}-tumor-bearing mice treated with saline were also imaged and analyzed under the same experimental conditions as those for Figure 9A,B (Figure S7, Supporting Information).

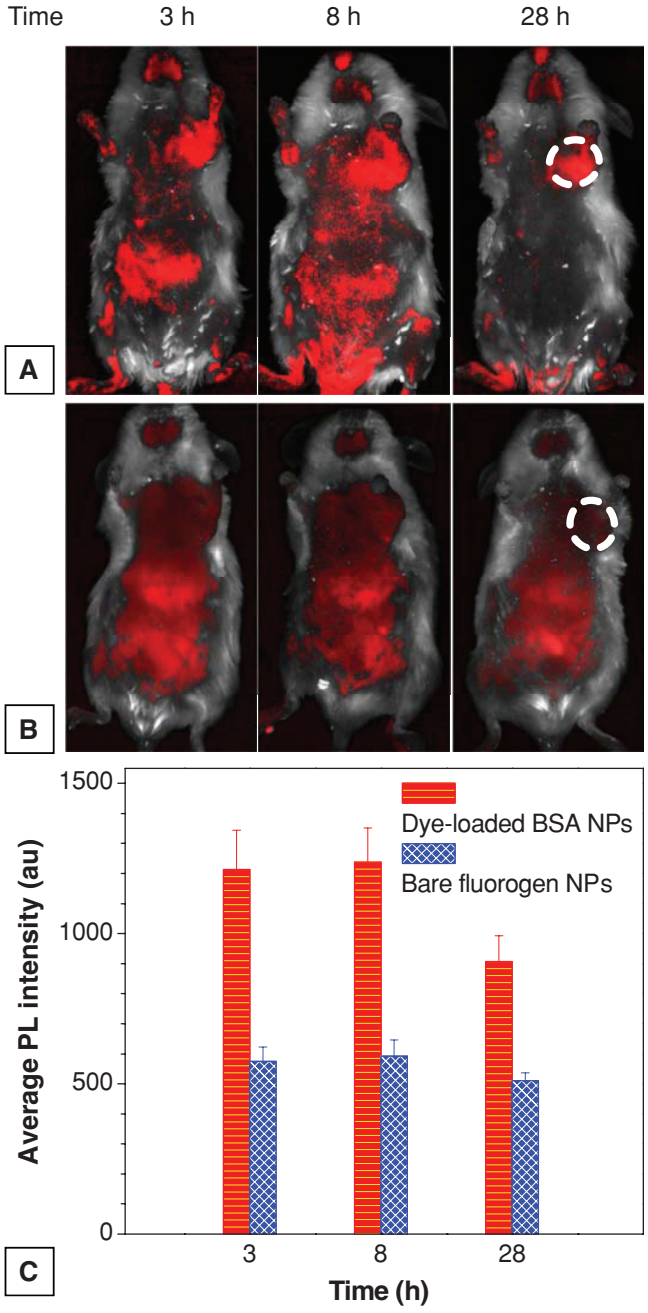

Figure 9. a,b) In vivo non-invasive fluorescence imaging of H_{22}-tumor-bearing mice after intravenous injection of fluorogen-loaded BSA NPs (with TPE-TPA-DCM loading of 0.86 wt%) (a) and bare TPE-TPA-DCM NPs (b) at the same fluorogen concentration. The white circles mark the tumor sites. c) Average PL intensities for the tumor tissues from the mice treated with the fluorogen-loaded BSA NPs and the bare fluorogen NPs at different times.

No fluorescence signals were observed after the removal of the mouse autofluorescence, which indicates that the fluorescence signals (red) in Figure 9A,B were indeed from the TPE-TPA-DCM-loaded BSA NPs and the bare TPE-TPA-DCM NPs, respectively. Figure 9C summarizes the semiquantitative analysis data of the average TPE-TPA-DCM fluorescence intensities

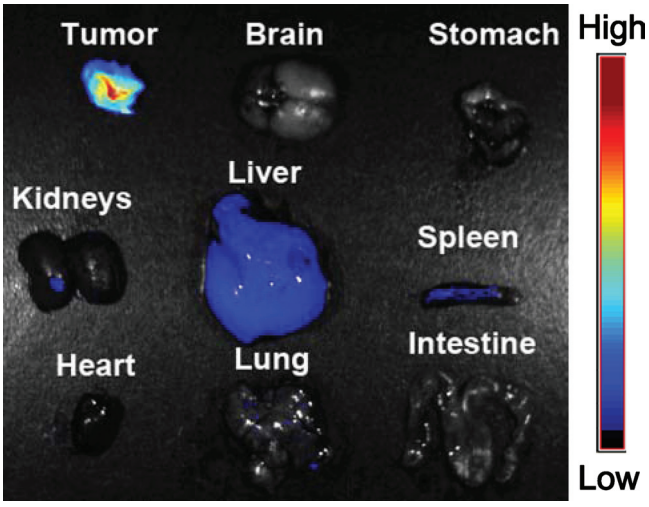

Figure 10. Ex vivo fluorescence imaging on tumor tissue and major organs of mice treated with AIE-fluorogen-loaded BSA NPs, which were sacrificed at 24 h post-injection. The tissue autofluorescence was removed by spectral unmixing software.

for tumor tissues from mice treated with the fluorogen-loaded BSA NPs and the bare TPE-TPA-DCM NPs. The average fluorescence intensities of the tumors stained by the fluorogen-loaded BSA NPs were nearly twice as high as those for the bare TPE-TPA-DCM NPs at all of the imaging time points, (i.e., 3, 8, and 28 h). Clearly, the BSA formulation favors enhanced accumulation of the AIE-active fluorogen-loaded BSA NPs in tumors, resulting in clear differentiation of the tumor from other tissues.

3. Conclusions

In summary, we have synthesized TPE-TPA-DCM, fabricated its BSA NPs, and explored their in vivo and in vitro bioimaging applications. The TPE-TPA-DCM possesses both TICT and AIE features, and its BSA-formulated NPs show efficient FR/NIR fluorescence with low cytotoxicity, uniform size and spherical morphology. As compared with the bare TPE-TPA-DCM NPs, the fluorogen-loaded BSA NPs show an increased cancer-cell uptake and a prominent tumor-targeting capability by the EPR effect on the H_{22}-tumor-bearing mouse model, clearly demonstrating the great potential of the BSA-formulated AIE-active NPs as an FR/NIR fluorescent probe for in vitro and in vivo imaging. This study thus opens up a new avenue for the development of AIE-active, biocompatible, NP-based probes for cancer imaging and diagnostics.

4. Experimental Section

Materials: The malononitrile derivative, **2**,[15] the TPE derivative, **3**,[17] 4-(diphenylamino)benzaldehyde[16] and 4-((4-bromophenyl)(phenyl)amino)benzaldehyde[16] were prepared according to the reported experimental procedures. BSA, glutaraldehyde, penicillin-streptomycin solution, trypsin-ethylenediaminetetra-acetic acid (EDTA) solution, MTT and DAPI were purchased from Sigma–Aldrich (St. Louis, USA). The

fetal bovine serum (FBS) was purchased from Gibco (Lige Technologies, Switzerland). Acetonitrile was distilled over P_2O_5. THF was distilled from sodium benzophenone ketyl under dry nitrogen immediately prior to use. Milli-Q water was supplied by a Milli-Q Plus System (Millipore Corp., Breford, USA). The MCF-7 breast-cancer cells were obtained from the American Type Culture Collection. The murine hepatic H_{22} cancer cells were purchased from the Shanghai Institute of Cell Biology (Shanghai, China). Male ICR mice (6–8 weeks old) were provided by the animal center of Drum-Tower Hospital (Nanjing, China).

Characterization: The ^{1}H- and ^{13}C-NMR spectra were recorded using a Bruker AV 300 spectrometer, in $CDCl_3$, using tetramethylsilane (TMS) (δ = 0) as an internal reference. The high-resolution mass spectra (HRMS) were recorded using a GCT premier CAB048 mass spectrometer operating in matrix-assisted laser desorption ionization time-of-flight (MALDI-TOF) mode. The absorption spectra were recorded using a Shimadzu UV-1700 spectrometer. The emission spectra were recorded using a Perkin–Elmer LS 55 spectrofluorometer. The average particle size and the size distribution of the NPs were measured by LLS, using a 90Plus particle-size analyzer (Brookhaven Instruments Co., USA) at a fixed angle of 90° and at room temperature. The zeta potential of the NPs was measured using a Brookhaven ZetaPlus zeta-potential analyzer at room temperature. The morphology of the NPs was studied using FE-SEM (JSM-6700F, JEOL, Japan) at an accelerating voltage of 10 kV. The samples were fixed on a stub with double-sided sticky tape and then coated with a platinum layer using an autofine coater (JEOL, Tokyo, Japan) for 60 s in a vacuum at a current intensity of 10 mA. The morphology of the NPs was also investigated by TEM (JEM-2010F, JEOL, Japan).

Synthesis of TPE-TPA-DCM: The fluorogen was prepared according to Scheme 1. $Pd(PPh_3)_4$ (36 mg) was added into a stirred mixture of 336 mg (0.4 mmol) of Br-TPA-DCM, 526 mg (1.4 mmol) of **3** and 1060 mg of K_3PO_4 (5 mmol) in 50 mL of THF and 8 mL of water under nitrogen. The mixture was heated to 70 °C for 36 h. After cooling to room temperature, the solution was extracted with dichloromethane (100 mL) twice, washed with water and dried over Na_2SO_4. After filtration and solvent evaporation under reduced pressure, the product was purified by silica-gel column chromatography using hexane/dichloromethane as the eluent. TPE-TPA-DCM was obtained in a 60% yield (322 mg) as a red powder after recrystallization from a mixture of chloroform/isopropyl alcohol. ^{1}H NMR (300 MHz, $CDCl_3$, δ): 7.51–7.40 (m, 10H), 7.35–7.29 (m, 8H), 7.17–7.01 (m, 48H), 6.63 (s, 2H; pyran H), 6.60 (d, J = 16 Hz, 2H; pyran –CH=); ^{13}C NMR (75 MHz, $CDCl_3$, δ): 159.39, 156.53, 150.50, 147.26, 146.54, 144.41, 144.39, 144.37, 143.40, 141.83, 141.15, 138.59, 138.07, 136.97, 132.55, 132.03, 130.29, 129.75, 128.34, 127.16, 126.44, 126.27, 126.14, 125.08, 122.50, 116.51, 116.35, 107.07, 58.96; HRMS (MALDI-TOF, m/z): $[M]^+$ calcd for $C_{100}H_{70}N_4O$, 1343.5583; found, 1343.5820. Anal. calcd for $C_{100}H_{70}N_4O$: C 89.39, H 5.25, N 4.17; found: C 89.66, H 5.23, N, 4.22.

Fabrication of Fluorogen-Loaded BSA NPs: The BSA NPs loaded with TPE-TPA-DCM were prepared by a modified desolvation method. The NPs were prepared with varied feeding ratios ranging from 0.25 to 5 wt%, defined as the ratio of the weight of the fluorogen to that of the BSA in the feed mixture. In brief, 13 mg of BSA were dissolved in 5 mL of Milli-Q water. Subsequently, 8 mL of THF (desolvation agent) containing a predetermined amount of TPE-TPA-DCM were added dropwise into the aqueous solution of BSA under sonication at room temperature, using a microtip probe sonicator with an 18 W output (XL2000, Misonix Incorp., USA), leading to the formation of the fluorogen-loaded BSA NPs. A small amount (5 μL) of glutaraldehyde solution (50%) was then added to cross-link the NPs at room temperature for 4 h. The THF was removed by rotary evaporation under vacuum. The cross-linked fluorogen-loaded BSA-NP suspension was filtered through a 0.45 μm microfilter and was then washed with Milli-Q water. The amounts of the fluorogen aggregates successfully encapsulated into the BSA NPs were determined from the absorption spectra with reference to a calibration curve established from dimethyl sulfoxide (DMSO) solutions of TPE-TPA-DCM. The EE is defined as the ratio of the amount of the fluorogen aggregates loaded in the NPs to the total amount of the fluorogen in the feed mixture. To prepare the bare TPE-TPA-DCM NPs, 60 μL of a THF solution of the fluorogen (0.5 mg mL^{-1}) were added into 3 mL of a water/THF (9:1 v/v) mixture, followed by sonication of the fluorogen mixture for 60 s at an 18 W output. The emulsion was then stirred at room temperature overnight to evaporate the THF solvent.

Cell Culture: The MCF-7 breast-cancer cells and the murine hepatic H_{22} cancer cells were cultured in Dulbecco's modified Eagle's medium (DMEM) containing 10% fetal bovine serum and 1% penicillin streptomycin at a constant temperature of 37 °C in a humidified environment containing 5% CO_2. Prior to the imaging experiments, the cells were precultured until confluence was reached.

Cell Imaging: The MCF-7 cells were cultured in a LAB-TEK chamber (Chambered Coverglass System, Rochester, USA) at 37 °C. After 80% confluence, the medium was removed and the adherent cells were washed twice with 1 × phosphate buffered saline (PBS) buffer. The AIE-active fluorogen-loaded BSA NPs (with a fluorogen loading of 0.86 wt%) or the bare TPE-TPA-DCM NPs (0.4×10^{-6} M) in FBS-free DMEM were then added to the chamber. After incubation for 2 h, the cells were washed three times with 1 × PBS buffer and then fixed with 75% ethanol for 20 min, followed by further washing, twice with 1 × PBS buffer. The nuclei were stained by DAPI for 10 min. The cell monolayer was then washed twice with 1 × PBS buffer and imaged by CLSM (Zeiss LSM 410, Jena, Germany) using the Olympus Fluoview FV1000 imaging software. The fluorescent signals from the NPs were collected upon excitation at 488 nm (1.25 mW) with a 650 nm long-pass barrier filter. To study the photostability of the AIE-active fluorogen-loaded BSA NPs in a biological environment, CLSM images of NP-stained MCF-7 cancer cells were recorded at 2 min intervals under continuous laser scanning at an excitation wavelength of 488 nm (1.25 mW). The fluorescence intensity of each image was analyzed using the Image Pro Plus software. The photostability of the NPs was expressed by the ratio of the fluorescence intensity, after excitation for a designated time interval, to its initial value as a function of exposure time. As a control, the photostability of fluorescein isothiocyanate in the MCF-7 cancer cells was also studied following the same procedures.

Cytotoxicity of Fluorogen-Loaded BSA NPs: The cytotoxicity of the NPs against MCF-7 breast-cancer cells was assessed by MTT assay. In brief, MCF-7 cells were seeded in 96-well plates (Costar, IL, USA) at a density of 4×10^4 cells mL^{-1}. After 24 h incubation, the cells were exposed to a series of doses of fluorogen-loaded BSA NPs at 37 °C. To eliminate the UV-absorption interference of the fluorogen-loaded NPs at 570 nm, the cells were incubated with the same series of doses of the fluorogen-loaded NPs as the control. After the designated time intervals, the sample wells were washed twice with 1 × PBS buffer, and 100 μL of freshly prepared MTT solution (0.5 mg mL^{-1}) in culture medium were added into each sample well. The MTT-medium solution was carefully removed after 3 h incubation in the incubator for the sample wells, whereas the control wells without the addition of MTT solution were washed twice with 1 × PBS buffer. DMSO (100 μL) was then added into each well and the plate was gently shaken for 10 min at room temperature to dissolve all of the precipitates formed. The absorbance of individual wells at 570 nm was then monitored using a Tecan GENios Microplate Reader. The absorbance of MTT in the sample well was determined by the differentiation between the absorbance of the sample well and that of the corresponding control well. The cell viability was expressed by the ratio of the absorbance of MTT in the sample wells to that of the cells incubated with culture medium only.

In Vivo Real-Time Fluorescence Imaging: All of the animal studies were performed in compliance with guidelines set by the Animal Care Committee at Drum-Tower Hospital. An H_{22}-cell suspension containing $5–6 \times 10^6$ cells (0.1 mL) was injected subcutaneously into the ICR mice (average body weight of 25 g) at the left axilla. When the tumor volume reached a mean size of about 400 mm^3, the mice were intravenously injected with 250 μL of the fluorogen-loaded BSA NPs (with a fluorogen loading of 0.86 wt%) at an NP concentration of 1 mg mL^{-1}. Similar experiments were conducted with the bare TPE-TPA-DCM NPs at the same fluorogen concentration. The mice were anesthetized and placed on an animal plate heated to 37 °C. The time-dependent biodistribution

in the mice was imaged using a Maestro in vivo fluorescence-imaging system (CRi, Inc., Woburn, USA). Light with a central wavelength of 523 nm was selected as the excitation source. In vivo spectral imaging from 560 to 900 nm (with 10 nm steps) was conducted, with an exposure time of 150 ms for each image frame. Autofluorescence was removed using spectral unmixing software. After removing the autofluorescence, the average TPE-TPA-DCM fluorescence intensity in the tumor tissue was calculated from the unmixed signal images using the region-of-interest (ROI) function of the Maestro software. Scans were carried out at 3 h, 8 h and 28 h post-injection. Moreover, the H_{22}-tumor-bearing mice were also sacrificed at 24 h post-intravenous injection of the AIE-fluorogen-loaded BSA NPs. The organs, including the brain, stomach, kidneys, liver, spleen, heart, lung and the intestines, and the tumor were excised and imaged using the Maestro system for ex vivo fluorescence imaging.

Supporting Information

Supporting Information is available from the Wiley Online Library or from the author.

Acknowledgements

W.Q and D.D contributed equally to this work. The authors are grateful to support from the Singapore National Research Foundation (R-279-000-323-281), the Research Grants Council of Hong Kong (603509 and HKUST2/CRF/10), the Temasek Defence Systems Institute of Singapore (R279-000-305-592/422/232), the Institute of Materials Research and Engineering of Singapore (IMRE/11-1C0213), the Innovation and Technology Commission of Hong Kong (ITP/008/09NP), the University Grants Committee of Hong Kong (AoE/P-03/08), an NSFC/RGC grant (N_HKUST620/11) and the National Science Foundation of China (20974028 and 21074051).

Received: September 15, 2011
Published online: December 9, 2011

[1] a) X. H. Gao, Y. Y. Cui, R. M. Levenson, L. W. K. Chung, S. M. Nie, *Nat. Biotechnol* **2004**, *22*, 969; b) C. Li, J. S. Xia, X. B. Wei, H. H. Yan, Z. Si, S. H. Ju, *Adv. Funct. Mater.* **2010**, *20*, 2222; c) Y. Kong, H. Q. Yao, H. J. Ren, S. Subbian, S. L. G. Cirillo, J. C. Sacchettini, J. H. Rao, J. D. Cirillo, *Proc. Natl. Acad. Sci. USA* **2010**, *107*, 12239; d) X. Lin, J. Xie, L. Zhu, S. Lee, G. Niu, Y. Ma, K. Kim, X. Y. Chen, *Angew. Chem.* **2011**, *123*, 1607.

[2] a) C. K. Lim, S. Kim, I. C. Kwon, C. H. Ahn, S. Y. Park, *Chem. Mater.* **2009**, *21*, 5819; b) B. Law, C. H. Tung, *Bioconjugate Chem.* **2009**, *20*, 1683; c) K. Y. Pu, K. Li, B. Liu, *Adv. Funct. Mater.* **2010**, *20*, 2770; d) D. Ding, K. Li, Z. S. Zhu, K. Y. Pu, Y. Hu, X. Q. Jiang, B. Liu, *Nanoscale* **2011**, *3*, 1997.

[3] a) J. H. Kim, Y. S. Kim, K. Park, S. Lee, H. Y. Nam, K. H. Min, H. G. Jo, J. H. Park, K. Choi, S. Y. Jeong, R. W. Park, I. S. Kim, K. Kim, I. C. Kwon, *J. Controlled Release* **2008**, *127*, 41; b) K. Yang, S. Zhang, G. X. Zhang, X. M. Sun, S. T. Lee, Z. Liu, *Nano Lett.* **2010**, *10*, 3318.

[4] X. K. Shu, A. Royant, M. Z. Lin, T. A. Aguilera, V. Lev-Ram, P. A. Steinbach, R. Y. Tsien, *Science* **2009**, *324*, 804.

[5] a) B. Ballou, B. C. Lagerholm, L. A. Ernst, M. P. Bruchez, A. S. Waggoner, *Bioconjugate Chem.* **2004**, *15*, 79; b) X. Michalet, F. F. Pinaud, L. A. Bentolila, J. M. Tsay, S. Doose, J. J. Li, G. Sundaresan, A. M. Wu, S. S. Gambhir, S. Weiss, *Science* **2005**, *307*, 538.

[6] a) U. Resch-Genger, M. Grabolle, S. Cavaliere-Jaricot, R. Nitschke, T. Nann, *Nat. Methods* **2008**, *5*, 763; b) K. Li, J. Pan, S. S. Feng, A. W. Wu, K. Y. Pu, Y. T. Liu, B. Liu, *Adv. Funct. Mater.* **2009**, *19*, 3535.

[7] a) A. M. Derfus, W. C. W. Chan, S. N. Bhatia, *Nano Lett.* **2004**, *4*, 11; b) A. M. Smith, H. Duan, A. M. Mohs, S. Nie, *Adv. Drug Delivery Rev.* **2008**, *60*, 1226.

[8] a) S. Santra, J. S. Xu, K. M. Wang, W. H. Tan, *J. Nanosci. Nanotechnol.* **2004**, *4*, 590; b) S. Kim, H. E. Pudavar, A. Bonoiu, P. N. Prasad, *Adv. Mater.* **2007**, *19*, 3791; c) W. C. Wu, C. Y. Chen, Y. Q. Tian, S. H. Jang, Y. N. Hong, Y. Liu, R. R. Hu, B. Z. Tang, Y. T. Lee, C. T. Chen, W. C. Chen, A. K. Y. Jen, *Adv. Funct. Mater.* **2010**, *20*, 1413; d) F. Mahtab, Y. Yu, J. W. Y. Lam, J. Z. Liu, B. Zhang, P. Lu, X. X. Zhang, B. Z. Tang, *Adv. Funct. Mater.* **2011**, *21*, 1733; e) K. Li, Y. H. Jiang, D. Ding, X. H. Zhang, Y. T. Liu, J. L. Hua, S. S. Feng, B. Liu, *Chem. Commun.* **2011**, 7323.

[9] J. B. Birks, *Photophysics of Aromatic Molecules*, Wiley, London, UK **1970**.

[10] a) J. D. Luo, Z. L. Xie, J. W. Y. Lam, L. Cheng, H. Y. Chen, C. F. Qiu, H. S. Kwok, X. W. Zhan, Y. Q. Liu, D. B. Zhu, B. Z. Tang, *Chem. Commun.* **2001**, 1740; b) Z. Zhao, Z. Wang, P. Lu, C. Y. K. Chan, D. Liu, J. W. Y. Lam, H. H. Y. Sung, I. D. Williams, Y. Ma, B. Z. Tang, *Angew. Chem. Int. Ed.* **2009**, *48*, 7608; c) Y. Liu, Y. Tang, N. N. Barashkov, I. S. Irgibaeva, J. W. Y. Lam, R. Hu, D. Birimzhanova, Y. Yu, B. Z. Tang, *J. Am. Chem. Soc.* **2010**, *132*, 13951; d) Y. Liu, C. Deng, L. Tang, A. Qin, R. Hu, J. Z. Sun, B. Z. Tang, *J. Am. Chem. Soc.* **2011**, *133*, 660.

[11] a) Y. N. Hong, J. W. Y. Lam, B. Z. Tang, *Chem. Soc. Rev.* **2011**, *40*, 5361; b) Z. Zhao, J. W. Y. Lam, B. Z. Tang. *Curr. Org. Chem.* **2010**, *14*, 2109; c) Y. N. Hong, J. W. Y. Lam, B. Z. Tang, *Chem. Commun.* **2009**, 4332; d) J. Liu, J. W. Y. Lam, B. Z. Tang, *J. Inorg. Organomet. Polym. Mater.* **2009**, *19*, 249.

[12] a) W. Z. Yuan, P. Lu, S. M. Chen, J. W. Y. Lam, Z. M. Wang, Y. Liu, H. S. Kwok, Y. G. Ma, B. Z. Tang, *Adv. Mater.* **2010**, *22*, 2159; b) Z. J. Zhao, S. M. Chen, J. W. Y. Lam, P. Lu, Y. C. Zhaong, K.S. Wong, H. S. Kwok, B. Z. Tang, *Chem. Commun.* **2010**, *46*, 2221; c) Z. Zhao, P. Lu, J. W. Y. Lam, Z. Wang, C. Y. K. Chan, H. H. Y. Sung, I. D. Williams, Y. Ma, B. Z. Tang, *Chem. Sci.* **2011**, *2*, 672.

[13] Y. Zhu, W. J. Tong, C. Y. Gao, H. Möhwald, *J. Mater. Chem.* **2008**, *18*, 1153.

[14] T. Tanaka, S. Shiramoto, M. Miyashita, Y. Fujishima, Y. Kaneo, *Int. J. Pharm.* **2004**, *277*, 39.

[15] L. L. Woods, *J. Am. Chem. Soc.* **1958**, *80*, 1442.

[16] a) K. P. Li, J. L. Qu, B. Xu, Y. H. Zhou, L. J. Liu, P. Peng, W. J. Tian, *New J. Chem.* **2009**, *33*, 2120; b) B. Wei, J. Z. Liu, Y. Zhang, J. H. Zhang, H. N. Peng, H. L. Fan, Y. B. He, X. C. Gao, *Adv. Funct. Mater.* **2010**, *20*, 2448; c) J. H. Kim, M. H. You, H. Lee, *J. Polym. Sci., Part A: Polym. Chem.* **2006**, *44*, 3729.

[17] Z. J. Zhao, S. M. Chen, J. W. Y. Lam, P. Lu, Y. C. Zhong, K. S. Wong, H. S. Kwok, B. Z. Tang, *Chem. Commun.* **2010**, 2221.

[18] R. R. Hu, E. Lager, A. Aguilar-Aguilar, J. Z. Liu, J. W. Y. Lam, H. H. Y. Sung, I. D. Williams, Y. C. Zhong, K. S. Wong, E. Pena-Cabrera, B. Z. Tang, *J. Phys. Chem. C* **2009**, *113*, 15845.

[19] S. D. Li, L. Huang, *Mol. Pharmceut.* **2008**, *5*, 496.

[20] a) H. Cabral, N. Nishiyama, S. Okazaki, H. Koyama, K. Kataoka, *J. Controlled Release* **2005**, *101*, 223; b) Z. Liu, K. Chen, C. Davis, S. Sherlock, Q. Cao, X. Y. Chen, H. J. Dai, *Cancer Res.* **2008**, *68*, 6652; c) V. Torchilin, *Eur. J. Pharm. Biopharm.* **2009**, *71*, 431.

[21] Z. Liu, C. Davis, W. B. Cai, L. He, X. Y. Chen, H. J. Dai, *Proc. Natl. Acad. Sci. USA* **2008**, *105*, 1410.

[22] a) M. R. Dreher, W. G. Liu, C. R. Michelich, M. W. Dewhirst, F. Yuan, A. Chilkoti, *J. Natl. Cancer Inst.* **2006**, *98*, 335; b) L. E. van Vlerken, Z. F. Duan, S. R. Little, M. V. Seiden, M. M. Amiji, *Mol. Pharmaceutics* **2008**, *5*, 516; c) D. Ding, Z. S. Zhu, R. T. Li, X. L. Li, W. Wu, X. Q. Jiang, B. R. Liu, *ACS Nano* **2011**, *5*, 2520.

[23] L. Y. Zhang, M. Yang, Q. Wang, Y. Li, R. Guo, X. Q. Jiang, C. Z. Yang, B. R. Liu, *J. Controlled Release* **2007**, *119*, 153.